Evaluation of Breast Tumor Blood Flow with Dynamic First-Pass ^{18}F-FDG PET/CT: Comparison with Angiogenesis Markers and Prognostic Factors

Alexandre Cochet[1,2], Sophie Pigeonnat[3], Blandine Khoury[1], Jean-Marc Vrigneaud[1], Claude Touzery[1], Alina Berriolo-Riedinger[1], Inna Dygai-Cochet[1], Michel Toubeau[1], Olivier Humbert[1], Bruno Coudert[4], Pierre Fumoleau[4], Laurent Arnould[3], and François Brunotte[1,2]

[1]Department of Nuclear Medicine, Centre Georges-François Leclerc, Dijon, France; [2]LE2i CNRS UMR 5158, Dijon, France; [3]Department of Pathology, Centre Georges-François Leclerc, Dijon, France; and [4]Department of Oncology, Centre Georges-François Leclerc, Dijon, France

The purpose of this study was to prospectively evaluate the relationship between tumor blood flow and glucose metabolism as evaluated by dynamic first-pass ^{18}F-FDG PET and by proliferation and endothelial pathologic markers in the setting of newly diagnosed breast cancer. **Methods:** Forty patients were prospectively included. Biopsy samples of each tumor were used to assess the Ki67 index of proliferation and immunostaining for CD34 (a panendothelial cell marker) and CD105 (a proliferation-related endothelial cell marker). All patients underwent ^{18}F-FDG PET/CT at least 1 wk after sample biopsy and before any treatment. A dynamic 2-min acquisition was performed immediately after intravenous injection of a 5 MBq/kg dose of ^{18}F-FDG; tumor blood flow was then calculated using a single-compartment kinetic model. A static acquisition was performed 90 min after injection for quantification of delayed ^{18}F-FDG tumor uptake (standardized uptake value maximal index [SUV_{max}]), reflecting tumor metabolism. **Results:** Pathologic and PET/CT data were available for all patients. The SUV_{max} measured on delayed PET images correlated strongly and positively with the expression of Ki67 ($r = +0.69$; $P < 0.0001$). In contrast, there was no significant correlation between SUV_{max} and endothelial markers (CD34 and CD105). Tumor blood flow correlated positively with the expression of CD34 and CD105 ($P = 0.016$ and $P = 0.007$, respectively) and with the expression of Ki67 ($P = 0.028$). By logistic regression analysis, only expression of Ki67 remained an independent predictor of high (supramedian) SUV_{max}; CD105 score and histopathologic grade 3 were independently associated with a high (supramedian) tumor blood flow level. **Conclusion:** Tumor blood flow quantified by dynamic first-pass ^{18}F-FDG PET/CT is significantly associated with tumor angiogenesis as evaluated by immunohistochemistry in the setting of breast cancer, whereas tumor metabolism appears to be more associated with markers of proliferation. Thus, determination of tumor blood flow and metabolism with a single injection of ^{18}F-FDG could be an exciting alternative to more complex and less available techniques.

Key Words: breast cancer; ^{18}F-FDG; blood flow; angiogenesis

J Nucl Med 2012; 53:512–520
DOI: 10.2967/jnumed.111.096834

Breast cancer is the most commonly diagnosed cancer in women and is the primary cause of death by cancer for women in the western world. Because of the Warburg effect (*1*), breast tumors are typically associated with an increase in tumor blood flow due to angiogenesis and an increase in glucose metabolism, but glucose metabolism and blood flow are often mismatched in breast cancer (*2*). Moreover, a flow–metabolism mismatch (high glucose metabolism relative to blood flow) is associated with poor response to systemic therapy and early relapse or disease progression (*3,4*). Thus, determination of these 2 key parameters is essential in characterizing the aggressiveness of breast tumors.

PET/CT with ^{18}F-FDG is the gold standard for in vivo evaluation of tumor glucose metabolism and is widely used in clinical oncology. In the setting of breast cancer, ^{18}F-FDG uptake has also been found to correlate with markers of proliferation, such as Ki67 (*5,6*). A range of techniques is available for tumor perfusion imaging, but the reference technique remains PET with ^{15}O-water (*7*). The 2-min half-life of ^{15}O permits evaluation of perfusion to be followed immediately by evaluation of metabolism with ^{18}F-FDG. However, because of this short half-life, only a few research centers with a cyclotron on site are able to use ^{15}O-water.

Almost 30 y ago, Mullani et al. developed a first-pass model for in vivo calculation of blood flow (*8*). This model was first used to evaluate myocardial perfusion with ^{82}Rb but was recently applied to the evaluation of tumor blood flow using ^{18}F-FDG and showed an excellent correlation with tumor blood flow measured with ^{15}O-water (*9*).

Immunohistochemical staining measurement of angiogenesis with antibodies to CD34 and CD105 can be used to

Received Sep. 20, 2011; revision accepted Nov. 18, 2011.
For correspondence or reprints contact: Alexandre Cochet, Department of Nuclear Medicine, Centre Georges-François Leclerc, 1 rue Professeur Marion, 21079 Dijon Cedex, France.
E-mail: acochet@cgfl.fr
Published online Sep. 17, 2012.

evaluate tumor vascularization (*10*). CD34 is a panendothelial marker that accurately reflects the degree of vascularization, whereas CD105 is a proliferation-related endothelial marker (*11*).

Thus, the objective of our study was to prospectively evaluate the relationship between tumor blood flow and glucose metabolism as evaluated by dynamic first-pass ^{18}F-FDG PET and by proliferation and endothelial pathologic markers in the setting of newly diagnosed breast cancer.

MATERIALS AND METHODS

Patients

From March 2009 to August 2010, 40 patients (mean age, 46 y; range, 27–72 y) with invasive breast cancer were prospectively recruited for ^{18}F-FDG PET/CT before any treatment. The inclusion criterion was newly diagnosed breast cancer, with primary tumor diameter larger than 2 cm. The exclusion criteria were pregnant or nursing patients, patients unwilling or unable to undergo serial imaging studies, and patients with inflammatory tumors. The clinical stage, determined according to the TNM classification of malignant tumors, was assessed by clinical examination, mammography, ultrasonography, pulmonary chest radiography, bone scintigraphy, and ^{18}F-FDG PET/CT. The local ethics review board gave permission for the study, and informed patient consent was obtained.

PET/CT Protocol

All imaging was performed using a PET/CT system (Gemini GXL; Philips) providing an axial field of view of 18 cm and a transaxial slice thickness of 4 mm. CT scans were used for anatomic registration with emission images but also for attenuation correction. Emission data, corrected for dead time, diffusion, and attenuation, were reconstructed with a fully 3-dimensional line-of-response–based iterative algorithm (*12*). Scans were performed at least 7 d after core biopsy (mean, 20 d; range, 7–36 d). All patients were instructed to fast for at least 6 h before the injection of ^{18}F-FDG. An intravenous cannula was placed in the arm, and a blood sample was drawn before ^{18}F-FDG injection for the determination of glycemia. Patients were positioned prone with both arms raised.

A bolus 5 MBq/kg injection of ^{18}F-FDG was administered using an automatic PET infusion system (Intego; Medrad) at a rate of 1 mL/s, immediately followed by a 30-mL injection of saline solution at the same rate. Simultaneously with the beginning of the injection, the first emission acquisition was started for 8 min (in list mode), with the breast centered in the axial field of view of the PET system (this position was previously determined on a scout view). A low-dose CT scan of the same region was then obtained (120 kVp, 120 mAs per slice, 0.5-s rotation time, 10 × 1.5 mm collimation, pitch of 0.7). Two different reconstruction parameters were applied to this acquisition: first, twelve 10-s frames were extracted from the first 2 min of the acquisition (dynamic first-pass images; Fig. 1). Second, a static reconstruction of the complete 8-min scan was performed (early static images; Fig. 1). Patients were then asked to rest for 50 min.

Sixty minutes after injection, a whole-body PET/CT scan was acquired from the brain to the upper thighs, with the patient supine. The CT scan was acquired before the PET scan, and the CT image data were then used to automatically position the patient for the PET acquisition. The emission acquisition time was 2 min per bed position, and the complete patient study typically involved 6–8 overlapping bed positions. The measured reconstructed transaxial spatial resolution for PET was 5.4 mm near the center of the field of view.

Finally, 90 min after injection, emission and transmission scans restricted to the chest (2 bed positions) were performed, with the patient prone and both arms raised (delayed static images; Fig. 1). The emission scan duration was 3 min for each bed position.

First-Pass Model for Measurement of Blood Flow

The concept of measuring tumor blood flow from the first pass of ^{18}F-FDG is based on the first-pass model of Mullani et al. (*8,9*). This model is based on the hypothesis that during the first transit of a bolus of activity through an organ (or a tumor), there exists a period during which the tracer has not left the region of interest, so that the venous concentration of the tracer is zero. This delay time (T_d) is longer with highly extracted tracers (*13*). Thus, on the basis of this assumption, if T is less than T_d, the tissue blood flow can be estimated using the following equation:

$$BF = \frac{Q(T)}{E.\int_0^T Ca(t)dt}, \qquad \text{Eq. 1}$$

where BF is the blood flow to the sampled tissue, Q(T) is the amount of the tracer in sampled tissue at any time T, *E* is the extraction fraction of the tracer in the sampled tissue, Ca(t) is the arterial concentration of the tracer at any time t, and dt is the variable of integration.

Mullani et al. compared the extraction fraction of ^{18}F-FDG in tumor tissue with the extraction fraction for the gold standard tracer ^{15}O-water (*9*). They found that ^{18}F-FDG extraction in tumors was close to ^{15}O-water extraction, averaging only 14% less. Thus, assuming that the extraction fraction of ^{18}F-FDG is close to 1, Equation 1 can be simplified to the following:

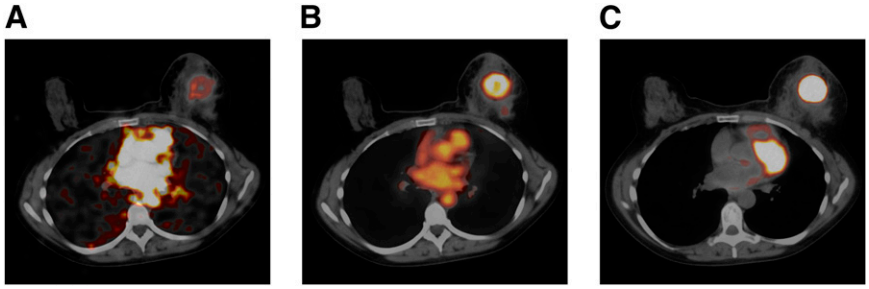

FIGURE 1. First-pass dynamic (A), early static (B), and delayed static (C) fused PET/CT images obtained, respectively, 30 s, 8 min, and 90 min after bolus injection of ^{18}F-FDG, in 57-y-old woman with TN invasive ductal carcinoma of left breast.

$$BF = \frac{Q(T)}{\int_0^T Ca(t)dt}. \quad \text{Eq. 2}$$

However, the error in flow measurement due to the statistical quality of the data can be minimized when both the numerator and the denominator in Equation 2 are determined at their maximum values (*8*). When T is less than T_d, the counting rate will reach a maximum when arterial input to the VOI ceases; both this input and the venous drainage are then zero, and the entire injected bolus is in the view of the detector, whose counting rate is momentarily steady, at maximum. Tumor blood flow can then be computed by dividing the peak counts by the first-pass arterial concentration integrated up to time T_m (peak-count time). The general first-pass flow equation can therefore be modified to the following peak-count flow equation:

$$BF = \frac{Q(T_m)}{\int_0^{Tm} Ca(t)dt}. \quad \text{Eq. 3}$$

Image and Data Analysis

PET/CT images were analyzed on a dedicated workstation (Extended Brilliance Workspace 3.5, with Syntegra software; Phillips).

For the determination of blood flow, the contours of the tumor were manually traced on each selected image, and then a volume of interest (VOI) was obtained by summing the results for each slice.

A second VOI of the same size was drawn on the contralateral normal breast, and a third VOI was drawn into the ascending aorta. These contours were defined using early PET images, corresponding CT images, and fused PET/CT images. In particular, the tumor VOI was adjusted to encompass the maximum available size of the lesion in all 3 planes. Other imaging modalities were not used in this process. Then, VOIs were superimposed onto the 10-s dynamic reconstruction PET images. From the dynamic PET images, time–activity curves were then obtained for the tumor, the contralateral breast, and the ascending aorta. The tumor time–activity curve was corrected for partial-volume effects as follows (*14*):

$$Q'(T) = \frac{(Q(T) - Bck(T))}{RC} + Bck(T), \quad \text{Eq. 4}$$

where Q′(T) is the partial-volume–corrected tumor activity at any time T in the tumor, Q(T) is the uncorrected activity at any time T in the tumor, Bck(T) is the background activity at any time T obtained from the contralateral normal breast VOI, and RC is the recovery coefficient. The recovery coefficients, which are equal to the measured activity concentration divided by the true activity concentration, were obtained from the analysis of hot-sphere phantoms (*14*). The volume of the tumor VOI was used to select the correct recovery coefficient value, using linear interpolation between values obtained from the sphere volumes included in the phantom measurements.

The peak count time (T_m) was determined visually on the arterial time–activity curve and defined as the end of the first pass of the tracer in the arterial VOI (*8*). Tumor blood flow was then calculated in mL/min/g of tumor, using Equation 3.

The standardized uptake value maximal index (SUV_{max}) of the tumor was measured on the delayed (90 min after injection) emission acquisition centered on the breast. A region of interest including the breast tumor was manually drawn on the slice with the highest radioactivity concentration. The SUV_{max} was corrected by body surface area and glycemia and normalized to standard body surface area (1.72 m^2) and normal glycemia (5.6 mmol/L):

$$SUV_{max} = \frac{C_{max} \times 70 \times BSA \times G}{IA \times 1.72 \times 5.6}, \quad \text{Eq. 5}$$

where C_{max} (Bq/mL) is the activity concentration in the voxel of highest tumor activity, IA (Bq) is the injected activity, G (mmol/L) is glycemia, and BSA is body surface area.

Histologic Preparation and Analysis

Tumor samples were collected by needle core biopsy. Tissue samples were fixed in 10% formalin and routinely processed for paraffin embedding. Histologic sections cut with 4-μm thickness were stained with hematoxylin, eosin, and safran.

Tumors were classified according to the method of the World Health Organization for carcinomas of the breast (*15*), and tumor grading was done in accordance with Elston and Ellis (*16*).

Immunohistochemistry was performed on 4-μm paraffin-embedded sections with an indirect immunoperoxidase method, using antibodies directed against estrogen receptor (ER), progesterone receptor (PR), human epidermal growth factor receptor 2 (*HER2*) oncoprotein, Ki67 protein, CD34 protein, and CD105 protein (ER: rabbit monoclonal prediluted antibody, clone SP1 [Ventana]; PR: rabbit monoclonal prediluted antibody, clone 1E2 [Ventana]; *HER2*: rabbit monoclonal prediluted antibody, clone 4B5 [Ventana]; Ki67: mouse monoclonal antibody, clone MIB-1 [Dako], in 1:50 dilution; CD34: mouse monoclonal antibody, clone QBEND 10 [Immunotech], in 1:200 dilution; CD105: mouse monoclonal antibody, clone SN6h [Dako], in 1:25 dilution). All immunostaining was performed on an automated immunostainer (BenchMark XT; Ventana).

ER and PR status were considered positive if the tumor showed at least 10% of cells to be positive using ER or PR antibody (*17*). *HER2* status was graded according to the HercepTest (Dako) scoring system modified by the recommendations of the American Society of Clinical Oncology and the College of American Pathologists (0, 1+, 2+, or 3+) (*18*). Tumors with scores of 3+ (i.e., strong homogeneous staining) were considered positive. If the score was 2+ (i.e., moderate complete membranous staining in ≥10% of tumor cells), fluorescent in situ hybridization was applied to confirm *HER2* amplification, using the dual-color *HER2* and CEN17 probes (ZytoLight SPEC *HER2*/CEN 17 Dual Color Probe kit; Zytovision GmbH). *HER2* amplification was defined, according to the criteria of the American Society of Clinical Oncology and the College of American Pathologists (*18*), by a *HER2*/CEN17 ratio of more than 2.2.

The percentage of Ki67-positive tumor cells was established for each sample. The number of vessels staining positively for CD34 or CD105 was counted on 10 consecutive fields at ×400 magnification in the area with carcinoma invasion. Vessels with a clearly defined lumen or well-defined linear vessel shape, but not single endothelial cells, were considered for microvessel assessment.

All analyses were done by 2 pathologists without knowledge of clinical, immunohistochemical, or imaging data.

Statistical Analysis

Continuous data were expressed as median (first quartile to third quartile), and qualitative data were expressed as numbers and

percentages. For continuous variables, normality of distribution was tested by the Kolmogorov–Smirnov test.

Spearman rank correlation was performed to analyze the relationship between SUV_{max}, blood flow, and histochemical biomarkers in the overall patient population ($n = 40$) and in the subpopulation of patients with non–triple-negative (non-TN) breast cancer ($n = 30$).

Differences in SUV_{max} and blood flow between menopausal status, tumor size, histologic grade, lymphovascular invasion, lymph node status, ER and PR status, *HER2* overexpression, and histochemical biomarkers (Ki67, CD34, and CD105) were tested using the nonparametric Mann–Whitney test or the Student *t* test, as appropriate.

Logistic regression analysis was performed to test for predictors that SUV_{max} would be over the median value (8.6) and that blood flow would be over the median value (0.32 mL/min/g). All variables listed in Table 1 were tested by univariate analysis. For multivariate analysis, all variables with a *P* value of less than 0.05 on univariate analysis were included in the model.

Patients were categorized into 3 groups according to ER, PR, and *HER2* expression. Group 1 included patients whose cancer was TN, lacking ER and PR expression and without *HER2* overexpression ($n = 10$). Group 2 included patients whose cancer was luminal, being positive for ER or PR and without *HER2* overexpression ($n = 15$). Group 3 included patients whose cancer was *HER2*+, having *HER2* overexpression but being either positive or negative for ER and PR ($n = 15$). Differences in SUV_{max}, blood flow, and the ratio of SUV_{max} to blood flow were tested among the 3 groups using a nonparametric Mann–Whitney test.

All tests were 2-sided, and a *P* value of less than 0.05 was considered significant.

Analyses were performed using the SPSS software package (version 13.0; SPSS Inc.).

RESULTS

^{18}F-FDG PET/CT was performed for all patients. The median tumor size was 36 mm (range, 21–100 mm). The clinical tumor stage was T2 for 24 patients (60%), T3 for 15 patients (38%), and T4a for 1 patient (2%). Invasive ductal carcinoma was diagnosed for 38 patients (96%); invasive lobular carcinoma was diagnosed for 2 patients (4%). Other tumor characteristics are shown in Table 1.

SUV_{max} and blood flow were available for all tumors. The average (±SD) SUV_{max} was 8.7 ± 5.5 (range, 1.6–23.4). The average blood flow was 0.32 ± 0.13 mL/min/g (range, 0.05–0.57 mL/min/g). The median peak count time (T_m) was 50 s (range, 30–70 s). In the overall patient population, there was a significant positive correlation between SUV_{max} and blood flow ($r = +0.35$, $P = 0.028$). There was also a strong positive correlation between SUV_{max} and Ki67 ($r = +0.69$, $P < 0.0001$) (Fig. 2). In contrast, there was no significant correlation between SUV_{max} and either CD34 score or CD105 score ($r = -0.11$ and $r = +0.27$, respectively, P = not statistically significant for either). There was a significant positive correlation between blood flow and CD34 score ($r = +0.38$, $P = 0.016$), between blood flow and CD105 score ($r = +0.43$, $P = 0.007$), and between blood flow and Ki67 ($r = +0.35$, $P = 0.028$).

TABLE 1
Comparison Between SUV_{max} and Blood Flow in the Patient and Clinical and Tumor Characteristics

			SUV_{max}			Blood flow (mL/min/g)		
Variable	Parameter	*n*	Median	Interquartile range	*P*	Median	Interquartile range	*P*
Menopausal	No	22 (55%)	6.7	5.2–9.9	0.48	0.31	0.23–0.38	0.72
	Yes	18 (45%)	6.8	5.0–14.5		0.32	0.20–0.43	
Tumor size	<5 cm	24 (60%)	6.8	5.3–10.2	0.50	0.33	0.21–0.38	0.29
	≥5 cm	16 (40%)	7.9	5.0–13.3		0.31	0.22–0.47	
Lymph node involvement	No	13 (32%)	5.4	3.9–13.0	0.54	0.28	0.20–0.39	0.40
	Yes	27 (68%)	7.9	5.5–11.7		0.33	0.23–0.42	
Histologic grade	1/2	26 (65%)	5.6	4.0–8.1	<0.001	0.27	0.20–0.37	0.030
	3	14 (35%)	13.3	8.5–16.3		0.39	0.32–0.46	
ER	−	14 (35%)	10.3	6.8–12.9	0.08	0.29	0.20–0.43	0.86
	+	26 (65%)	6.1	4.6–8.9		0.32	0.23–0.40	
PR	−	19 (48%)	9.2	6.5–12.7	0.021	0.36	0.25–0.42	0.18
	+	21 (52%)	5.5	3.1–9.3		0.28	0.20–0.38	
HER2	−	25 (63%)	9.3	4.5–13.0	0.60	0.28	0.20–0.45	0.64
	+	15 (37%)	6.5	5.5–8.1		0.33	0.27–0.38	
TN	Non-TN	30 (75%)	6.4	5.1–9.0	0.042	0.32	0.23–0.39	0.82
	TN	10 (25%)	11.9	10.2–14.2		0.23	0.18–0.45	
Lymphovascular invasion	No	6 (15%)	6.9	5.3–11.2	0.65	0.32	0.21–0.38	0.91
	Yes	34 (85%)	5.4	3.6–12.1		0.28	0.22–0.41	
Ki67 score	≤median	23 (58%)	5.7	3.5–7.0	<0.001	0.28	0.19–0.37	0.09
	>median	17 (42%)	12.1	7.9–14.6		0.38	0.25–0.45	
CD34 score	≤median	20 (50%)	7.7	4.6–12.6	0.57	0.24	0.17–0.38	0.027
	>median	20 (50%)	6.6	5.4–10.7		0.36	0.26–0.46	
CD105 score	≤median	20 (50%)	6.1	3.7–12.6	0.31	0.23	0.17–0.32	0.002
	>median	20 (50%)	7.5	6.4–11.9		0.37	0.32–0.44	

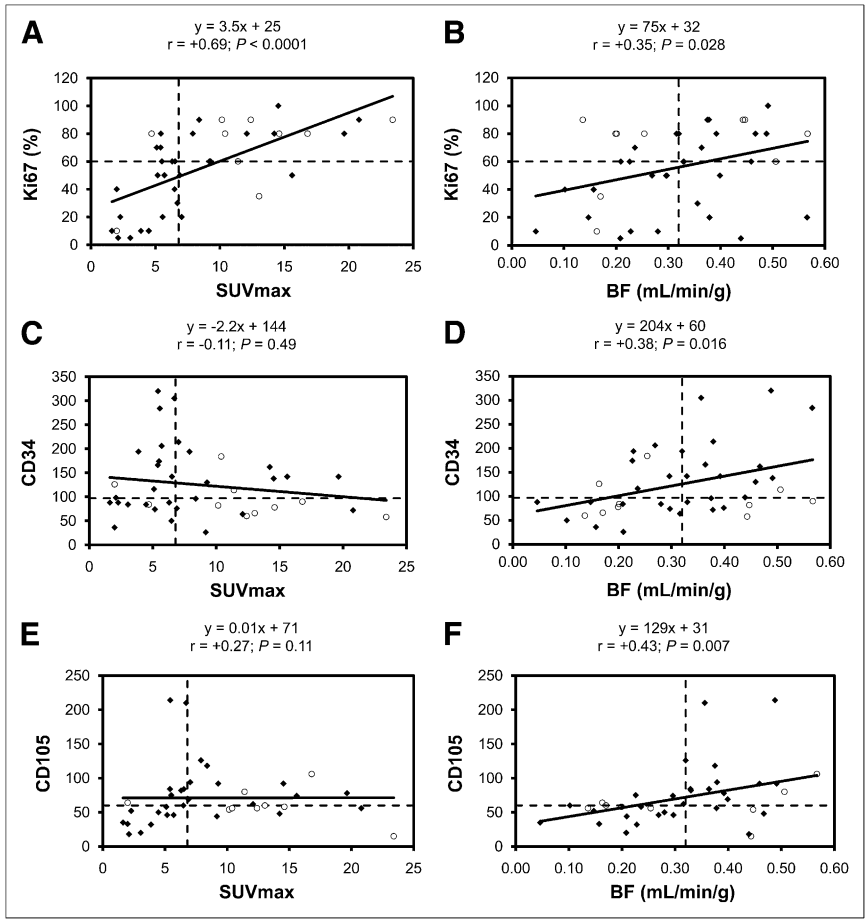

FIGURE 2. Spearman rank correlation with regression lines between SUV_{max} and Ki67 (A), tumor blood flow (BF) and Ki67 (B), SUV_{max} and CD34 (C), tumor blood flow and CD34 (D), SUV_{max} and CD105 (E), and tumor blood flow and CD105 (F). Horizontal and vertical dashed lines represent median value for each variable (6.8 for SUV_{max}, 60% for Ki67, 0.32 mL/min/g for blood flow, 97 for CD34, and 60 for CD105). ○ = TN breast tumors; ♦ = non-TN breast tumors.

In the subpopulation of patients with non-TN breast cancer, correlations were similar except that there was a significant positive correlation between SUV_{max} and CD105 score ($r = +0.50$, $P = 0.005$).

Table 1 shows the association between median SUV_{max} and blood flow, and clinical and tumor characteristics. Histopathologic grade 3 was associated with both higher SUV_{max} and higher blood flow, whereas PR status, TN tumor, and high (supramedian) Ki67 score were associated only with higher SUV_{max}. Finally, supramedian CD34 score and supramedian CD105 score were associated only with higher blood flow.

Logistic regression analysis was performed to test for predictors of high (supramedian) SUV_{max} (Table 2). By univariate analysis, the predictors of high SUV_{max} included histopathologic grade 3, TN breast cancer, and Ki67 score. By multivariate analysis, only Ki67 score remained an independent predictor of high SUV_{max}.

Logistic regression analysis was also performed to test for predictors of high (supramedian) values of blood flow (Table 3). By univariate analysis, the predictors of high blood flow included histopathologic grade 3, CD34 score, and CD105 score. By multivariate analysis, only histopathologic grade 3 and CD105 score remained independent predictors of high blood flow.

Functional imaging parameters by subtypes are shown in Figure 3. SUV_{max} differed by subtype, with a higher

TABLE 2
Predictors of High (Supramedian) SUV_{max} by Logistic Regression Analysis

	Univariate			Multivariate		
Predictor	OR	95% CI	*P*	OR	95% CI	*P*
Histopathologic grade 3	6.93	1.53–31.4	0.012	—	—	—
TN breast cancer	6.00	1.08–33.3	0.040	—	—	—
Ki67 score (%)	1.06	1.02–1.09	0.002	1.05	1.02–1.09	0.003

OR = odds ratio; CI = confidence interval.

TABLE 3
Predictors of High (Supramedian) Blood Flow by Logistic Regression Analysis

Predictor	Univariate			Multivariate		
	OR	95% CI	*P*	OR	95% CI	*P*
Histopathologic grade 3	6.93	1.53–31.4	0.012	9.56	1.60–57.2	0.013
CD34 score	1.01	1.00–1.02	0.046	—	—	—
CD105 score	1.05	1.01–1.09	0.011	1.05	1.01–1.09	0.021

OR = odds ratio; CI = confidence interval.

SUV_{max} for TN tumors than for other subtypes ($P = 0.042$). In contrast, there was no difference in blood flow among subtypes ($P = 0.82$). Finally, the metabolism-to-perfusion ratio (SUV_{max}/blood flow) was significantly higher in TN tumors than in other subtypes ($P = 0.02$).

DISCUSSION

In this prospective study, tumor blood flow assessed by dynamic first-pass ^{18}F-FDG PET/CT was shown to be significantly associated with microvessel density and angiogenesis as measured by immunohistochemistry markers (CD34 and CD105); in contrast, tumor metabolism assessed by delayed ^{18}F-FDG uptake was associated better with the marker of tumor proliferation (Ki67).

The recent success of targeted antiangiogenic therapy has increased the demand for imaging of tumor perfusion parameters and angiogenic cascade, in particular in the setting of breast cancer. Thus, a method for simultaneous measurement of tumor blood flow and metabolism may be an important addition for functional imaging of breast cancer. The technique developed by Mullani et al. is a simple 1-compartment flow model that estimates blood flow using only a 2-min scan (*8,9*). Together with delayed measure of SUV_{max}, this technique allows a simple evaluation of both perfusion and metabolism of the tumor after a single injection of ^{18}F-FDG, in contrast to more elaborate multiple-compartment models that require a long acquisition uncomfortable for the patient and long postprocessing procedures. As an illustration, previous studies found a close relationship between kinetic estimates of ^{18}F-FDG delivery (K_1) and blood flow (*19,20*). Moreover, in a recent study, a comparison of ^{18}F-FDG K_1 to standard breast cancer markers, including Ki67, yielded comparable results to our analysis of blood flow measures using dynamic ^{18}F-FDG PET (*21*).

Most microscopic studies of angiogenesis rely on histologic tissue sections. In such studies, blood vessel detection is improved by immunohistochemical staining of endothelial cell markers. CD34 (sialomucin) is expressed on mature vascular endothelial cells and circulating hematopoietic progenitor cells (*22*). CD105 (endoglin), the receptor for TGF-β, is also expressed by vascular endothelial cells but is upregulated in angiogenic vessels and accumulates preferentially in tumors (*23,24*). Thus, CD105 is considered a reference for immunochemistry bioassay of angiogenesis, whereas CD34 is more reflective of microvascular density, regardless of endothelial activation. The

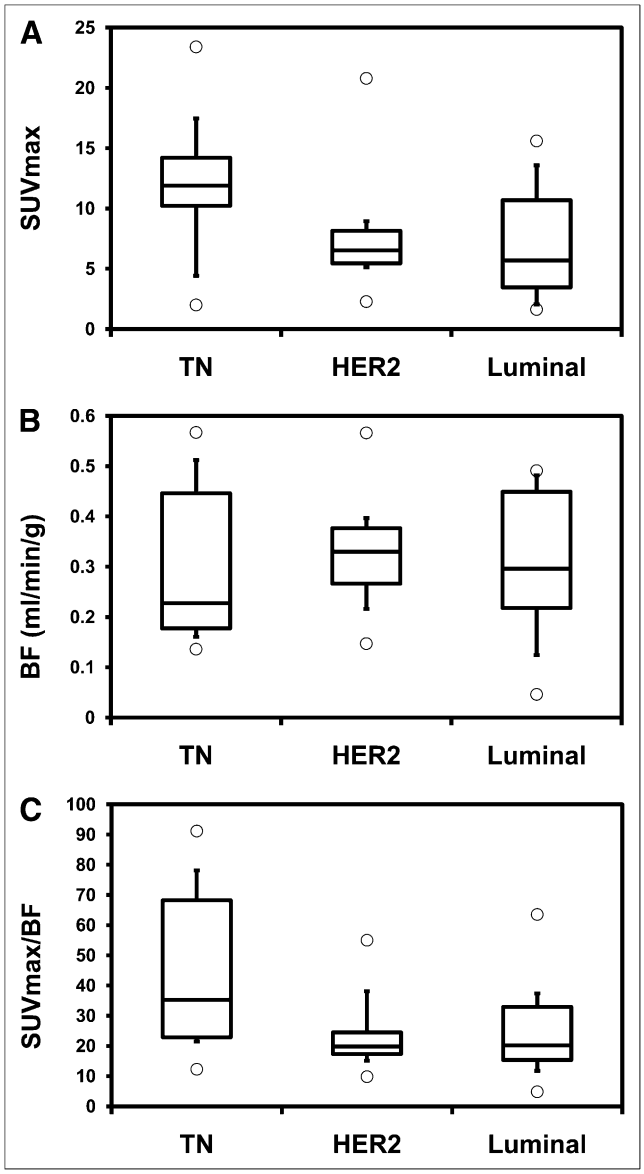

FIGURE 3. SUV_{max} (A), tumor blood flow (BF) (B), and SUV_{max}-to-blood flow ratio (C) according to subtypes.

expression of CD105 in breast cancer has also been demonstrated to be an independent predictor of survival (*25,26*). As a consequence, CD105 is regarded as a potential target for in vivo imaging of angiogenesis and for antiangiogenic therapy (*27,28*).

Our results show a significant correlation between tumor blood flow and expression of both CD34 and CD105. However, expression of CD34 failed to predict a high level of blood flow by multivariate analysis, whereas expression of CD105 remained an independent predictor of supramedian level of tumor blood flow. This difference may be explained by the fact that CD105 is expressed only by vascular endothelial cells in tumors whereas CD34 is also expressed by lymphatic endothelial cells (*29*). To our knowledge, there are very limited data in the literature regarding the relationship between tumor blood flow and expression of CD105. These findings underline the interest in tumor blood flow as a surrogate marker of angiogenesis, despite the potential discrepancy between total tumor blood flow as measured in our study and nutritive blood flow due to the aberrant tumor vasculature with vascular shunts (*30*).

Our results also confirm the strong relationship between proliferation as assessed by expression of Ki67 and glucose metabolism as determined by the measure of SUV_{max} in breast cancer. Previous studies also found a correlation between ^{18}F-FDG delayed uptake and expression of Ki67, in both TN and non-TN breast cancer (*5,6,31*). In contrast, we found a significant relationship between angiogenesis as assessed by CD105 and glucose metabolism in the subpopulation of patients with non-TN breast cancer but not in our entire cohort of patients. These findings agree with those reported by Groves et al., who found a positive correlation between CD105 and SUV_{max} in 20 patients with early-stage non-TN breast cancer (*32*). Concerning TN breast cancer, the higher rate of flow–metabolism mismatch observed in previous work and in our study could be an underlying cause of the inconsistent association between perfusion and metabolism in this particular subtype of tumor (*33*).

This study had some limitations. First, the simple 1-compartment flow model used in this study has some intrinsic limitations, well described by Mullani et al. (*9*). Briefly, the first pass of ^{18}F-FDG imaging may contain both free and trapped components of ^{18}F-FDG that can lead to an overestimation of blood flow due to increased extraction in tumor cells, in particular in tumors characterized by a high metabolic rate. However, the determination of peak-count time for each acquisition may minimize this phenomenon by shortening the time of acquisition used for the calculation of blood flow. On the other hand, an underestimation of high blood flow could occur because of the relatively limited first-pass extraction of ^{18}F-FDG, compared with ^{15}O-water, in that situation (*9*). However, despite these potential limitations, our estimates of tumor blood flow agree with values reported in previous studies, using ^{15}O-water, for comparable groups of patients (Table 4) (*19,20,34,35*).

Another potential limitation is the determination of transit time, since the peak-count time has been observed to be quite variable, depending on the flow rate (*7*). Thus, for high levels of tumor blood flow, transit time may be short and difficult to evaluate, with a time resolution of 10 s. The use of time-of-flight PET scanners may compensate for this issue in the future.

Finally, histologic examinations were performed on core biopsy samples and not on surgical specimens. Most of the patients included in this study had a large or locally advanced breast cancer and received neoadjuvant chemotherapy before surgery. As a consequence, it was impossible to evaluate histologic markers on surgical samples. Comparison of histologic markers evaluated on a sample of the tumor with functional imaging parameters determined for the whole tumor might be hampered by tumor heterogeneity. However, despite this limitation, we found a strong relationship between CD105 expression determined on biopsy samples and blood flow of the whole tumor. Moreover, CD105 evaluated on biopsy samples has been shown to predict clinical response to chemotherapy (*36*). In addition, even using surgical specimens, expression of CD105 is usually determined on the most vascular area of the tumor (hot spot) rather than on the whole tumor (*10*). We believe that it is essential to evaluate and compare histologic and functional parameters before surgery, since neoadjuvant therapy represents the best paradigm to assist the deployment of targeted anticancer agents, in particular antiangiogenic agents.

Our study raises several potential clinical implications. Antiangiogenic agents are now routinely used in various

TABLE 4
Studies Evaluating Tumor Blood Flow in Patients with Large or Locally Advanced Breast Cancer

Study	No. of patients	Tracer	Tumor blood flow (mL/min/g)	
			Mean ± SD	Range
Wilson et al. (1992) (*34*)	20	^{15}O-water	0.30 ± 0.17	0.11–0.77
Mankoff et al. (2002) (*35*)	37	^{15}O-water	0.32	
Zasadny et al. (2003) (*19*)	9	^{15}O-water	0.15 ± 0.08	0.08–0.29
Tseng et al. (2004) (*20*)	35	^{15}O-water	0.30	
Our study	40	^{18}F-FDG	0.32 ± 0.13	0.05–0.57

cancers even though their role in neoadjuvant therapy of breast cancer is still under evaluation (*37*). In this setting, evaluation of tumor blood flow with dynamic first-pass ^{18}F-FDG PET/CT may be an exciting alternative to less available techniques such as ^{15}O-water.

Simultaneous evaluation of tumor blood flow and glucose metabolism may also be of interest for monitoring cytotoxic chemotherapy and for prognostic stratification. Prior studies have shown that a low ratio of glucose metabolism to blood flow (evaluated with ^{15}O-water) is a good predictor of response to neoadjuvant chemotherapy, and of long-term survival, in patients with locally advanced breast cancer (*4,35*). A combined evaluation of both metabolism and perfusion may also identify subsets of tumors resistant to therapy. Specht et al. recently showed that a high metabolism-to-perfusion ratio, which predicts a poor response to neoadjuvant chemotherapy, was more common in TN breast tumors than in other subtypes (*33*). Using dynamic first-pass ^{18}F-FDG PET/CT to evaluate blood flow, we found similar results despite our more limited number of patients (Fig. 3), suggesting potential for this technique to obtain an accurate phenotype profile of breast tumors.

CONCLUSION

Tumor blood flow evaluated by dynamic first-pass ^{18}F-FDG PET/CT is highly significantly associated with angiogenesis as measured by CD105 expression in the setting of breast cancer, whereas glucose metabolism appears to be associated better with markers of proliferation. To develop the concept of personalized medicine, it is essential to obtain an accurate biologic and functional profile of tumors. In this respect, determination of tumor blood flow and metabolism with a single injection of ^{18}F-FDG may be an exciting alternative to more complex and less available techniques. Further investigations are needed to confirm the respective role of these 2 key parameters for elaboration of therapeutic strategies and response assessment in breast cancer.

DISCLOSURE STATEMENT

The costs of publication of this article were defrayed in part by the payment of page charges. Therefore, and solely to indicate this fact, this article is hereby marked "advertisement" in accordance with 18 USC section 1734.

ACKNOWLEDGMENTS

This study is part of the Pharmimage project. The authors thank the technologists from the Department of Nuclear Medicine of Centre Georges-François Leclerc, for their help in the development of this study. No potential conflict of interest relevant to this article was reported.

REFERENCES

1. Warburg O, Wind F, Negelein E. The metabolism of tumors in the body. *J Gen Physiol.* 1927;8:519–530.
2. Mankoff DA, Dunnwald LK, Partridge SC, Specht JM. Blood flow-metabolism mismatch: good for the tumor, bad for the patient. *Clin Cancer Res.* 2009;15:5294–5296.
3. Semple SI, Gilbert FJ, Redpath TW, et al. The relationship between vascular and metabolic characteristics of primary breast tumours. *Eur Radiol.* 2004;14:2038–2045.
4. Dunnwald LK, Gralow JR, Ellis GK, et al. Tumor metabolism and blood flow changes by positron emission tomography: relation to survival in patients treated with neoadjuvant chemotherapy for locally advanced breast cancer. *J Clin Oncol.* 2008;26:4449–4457.
5. Buck A, Schirrmeister H, Kuhn T, et al. FDG uptake in breast cancer: correlation with biological and clinical prognostic parameters. *Eur J Nucl Med Mol Imaging.* 2002;29:1317–1323.
6. Shimoda W, Hayashi M, Murakami K, Oyama T, Sunagawa M. The relationship between FDG uptake in PET scans and biological behavior in breast cancer. *Breast Cancer.* 2007;14:260–268.
7. Laking G, Price P. Radionuclide imaging of perfusion and hypoxia. *Eur J Nucl Med Mol Imaging.* 2010;37(suppl 1):S20–S29.
8. Mullani NA, Gould KL. First-pass measurements of regional blood flow with external detectors. *J Nucl Med.* 1983;24:577–581.
9. Mullani NA, Herbst RS, O'Neil RG, Gould KL, Barron BJ, Abbruzzese JL. Tumor blood flow measured by PET dynamic imaging of first-pass ^{18}F-FDG uptake: a comparison with ^{15}O-labeled water-measured blood flow. *J Nucl Med.* 2008;49:517–523.
10. Vermeulen PB, Gasparini G, Fox SB, et al. Second international consensus on the methodology and criteria of evaluation of angiogenesis quantification in solid human tumours. *Eur J Cancer.* 2002;38:1564–1579.
11. Weidner N. Tumoural vascularity as a prognostic factor in cancer patients: the evidence continues to grow. *J Pathol.* 1998;184:119–122.
12. Hu Z, Wang W, Gualtieri EE, et al. LOR-based fully-3D PET image reconstruction using a blob-basis function. In: *IEEE Medical Imaging Conference, 2007*. Piscataway, NJ: IEEE; 2007. Paper M26-228.
13. Zierler KL. Equations for measuring blood flow by external monitoring of radioisotopes. *Circ Res.* 1965;16:309–321.
14. Srinivas SM, Dhurairaj T, Basu S, Bural G, Surti S, Alavi A. A recovery coefficient method for partial volume correction of PET images. *Ann Nucl Med.* 2009;23:341–348.
15. Tavassoli FA, Devilee P. *Pathology and Genetics of Tumours of the Breast and Female Genital Organs*. Lyon, France: IARC Press; 2003:13–59.
16. Elston CW, Ellis IO. Pathological prognostic factors in breast cancer. I, the value of histological grade in breast cancer, experience from a large study with long-term follow-up. *Histopathology.* 1991;19:403–410.
17. Zafrani B, Aubriot MH, Mouret E, et al. High sensitivity and specificity of immunohistochemistry for the detection of hormone receptors in breast carcinoma: comparison with biochemical determination in a prospective study of 793 cases. *Histopathology.* 2000;37:536–545.
18. Wolff AC, Hammond ME, Schwartz JN, et al. American Society of Clinical Oncology/College of American Pathologists guideline recommendations for human epidermal growth factor receptor 2 testing in breast cancer. *J Clin Oncol.* 2007;25:118–145.
19. Zasadny KR, Tatsumi M, Wahl RL. FDG metabolism and uptake versus blood flow in women with untreated primary breast cancers. *Eur J Nucl Med Mol Imaging.* 2003;30:274–280.
20. Tseng J, Dunnwald LK, Schubert EK, et al. ^{18}F-FDG kinetics in locally advanced breast cancer: correlation with tumor blood flow and changes in response to neoadjuvant chemotherapy. *J Nucl Med.* 2004;45:1829–1837.
21. Dunnwald LK, Doot RK, Specht JM, et al. PET tumor metabolism in locally advanced breast cancer patients undergoing neoadjuvant chemotherapy: value of static versus kinetic measures of fluorodeoxyglucose uptake. *Clin Cancer Res.* 2011;17:2400–2409.
22. Pusztaszeri MP, Seelentag W, Bosman FT. Immunohistochemical expression of endothelial markers CD31, CD34, von Willebrand factor, and Fli-1 in normal human tissues. *J Histochem Cytochem.* 2006;54:385–395.
23. Duff SE, Li C, Garland JM, et al. CD105 is important for angiogenesis: evidence and potential applications. *FASEB J.* 2003;17:984–992.
24. Fonsatti E, Altomonte M, Nicotra MR, et al. Endoglin (CD105): a powerful therapeutic target on tumor-associated angiogenetic blood vessels. *Oncogene.* 2003;22:6557–6563.
25. Kumar S, Ghellal A, Li C, et al. Breast carcinoma: vascular density determined using CD105 antibody correlates with tumor prognosis. *Cancer Res.* 1999;59:856–861.
26. Dales JP, Garcia S, Bonnier P, et al. CD105 expression is a marker of high metastatic risk and poor outcome in breast carcinomas. Correlations between immunohistochemical analysis and long-term follow-up in a series of 929 patients. *Am J Clin Pathol.* 2003;119:374–380.

27. Dallas NA, Samuel S, Xia L, et al. Endoglin (CD105): a marker of tumor vasculature and potential target for therapy. *Clin Cancer Res.* 2008;14:1931–1937.
28. Hong H, Yang Y, Zhang Y, et al. Positron emission tomography imaging of CD105 expression during tumor angiogenesis. *Eur J Nucl Med Mol Imaging.* 2011;38:1335–1343.
29. Fiedler U, Christian S, Koidi S, et al. The sialomucin CD34 is a marker of lymphatic endothelial cells in human tumours. *Am J Pathol.* 2006;168:1045–1053.
30. Jain RK. Haemodynamic and transport barriers to the treatment of solid tumours. *Int J Radiat Biol.* 1991;60:85–100.
31. Tchou J, Sonnad SS, Bergey MR, et al. Degree of tumor FDG uptake correlates with proliferation index in triple negative breast cancer. *Mol Imaging Biol.* 2010;12:657–662.
32. Groves AM, Shastry M, Rodriguez-Justo M, et al. ^{18}F-FDG PET and biomarkers for tumour angiogenesis in early breast cancer. *Eur J Nucl Med Mol Imaging.* 2011;38:46–52.
33. Specht JM, Kurland BF, Montgomery SK, et al. Tumor metabolism and blood flow as assessed by positron emission tomography varies by tumor subtype in locally advanced breast cancer. *Clin Cancer Res.* 2010;16:2803–2810.
34. Wilson CB, Lammertsma AA, McKenzie CG, Sikora K, Jones T. Measurements of blood flow and exchanging water space in breast tumors using positron emission tomography: a rapid and noninvasive dynamic method. *Cancer Res.* 1992; 52:1592–1597.
35. Mankoff DA, Dunnwald LK, Gralow JR, et al. Blood flow and metabolism in locally advanced breast cancer: relationship to response to therapy. *J Nucl Med.* 2002;43:500–509.
36. Beresford MJ, Harris AL, Ah-See M, et al. The relationship of the neo-angiogenic marker, endoglin, with response to neoadjuvant chemotherapy in breast cancer. *Br J Cancer.* 2006;95:1683–1688.
37. Specht J, Gralow JR. Neoadjuvant chemotherapy for locally advanced breast cancer. *Semin Radiat Oncol.* 2009;19:222–228.